Anomalous Schottky Specific Heat and Structural Distortion in Ferromagnetic PrAl_{2}

Arjun K. Pathak, D. Paudyal, Y. Mudryk, K. A. Gschneidner, Jr., and V. K. Pecharsky

Phys. Rev. Lett. **110**, 186405 — Published 3 May 2013

DOI: 10.1103/PhysRevLett.110.186405

Anomalous Schottky specific heat and structural distortion in ferromagnetic $PrAl_2$

Arjun K. Pathak, [1,a] D. Paudyal, [1] Y. Mudryk, [1] K. A. Gschneidner, Jr., [1, 2] and V. K. Pecharsky[1, 2]

[1]The Ames Laboratory, U.S. Department of Energy, Iowa State University, Ames, Iowa 50011-3020, USA

[2]Department of Materials Science and Engineering, Iowa State University, Ames, Iowa 50011-2300, USA

Abstract

Unique from other rare earth dialuminides, $PrAl_2$ undergoes a cubic to tetragonal distortion below T = 30 K in a zero magnetic field, but the system recovers its cubic symmetry upon the application of an external magnetic field of 10 kOe via a lifting of the 4*f* crystal field splitting. The nuclear Schottky specific heat in $PrAl_2$ is anomalously high compared to that of pure Pr metal. First principles calculations reveal that the 4*f* crystal field splitting in the tetragonally distorted phase of $PrAl_2$ underpins the observed unusual low temperature phenomena.

PACS number(s): 61.50.Ks, 65.40.Ba, 71.20.Eh, 71.20.-b

[a] corresponding author: pathak138@ameslab.gov

Materials with structural transformations or distortions coupled to magnetic transitions show interesting magnetostrictive, magnetoresistive, and magnetocaloric behavior and are, therefore, important subject of study in condensed matter physics [1,2,3,4]. The importance of either coupled or decoupled magnetostructural transformations has been shown for many materials starting from high temperature superconductors [5] and perovskites [6] to multifunctional intermetallics [4], just to mention a few. The anomalies close to 0 K encompass another playground for the fundamental physics, and they range from the Kondo effect [7] and heavy fermion behavior [8] to quantum criticality [9] and nuclear Schottky specific heat [10]. These remarkable behaviors are ultimately related to the interplay between localized and delocalized electrons, for which lanthanides are truly the best model provided by nature. In particular, the rare earth dialuminides, which have simple cubic Laves phase structure at room temperature have long been the system of choice to understand the fundamentals of rare earth magnetism and low temperature anomalies.

Magnetism and crystallography of RAl_2 compounds (R = rare earth element) have been extensively studied over the last few decades, yet specific heat (C_p) and crystal structures of these systems at low temperature (LT), have not received much attention, thus creating a gap in understanding of the underlying fundamental physics of these materials. At room temperature, all of the RAl_2 compounds adopt cubic $MgCu_2$ Laves phase-type structure with space group $Fd\bar{3}m$ [11]. These dialuminides have been successfully employed for detailed studies of the crystal field (CF) effects that influence the

macroscopic physical properties such as specific heat, magnetic susceptibility, and electrical resistivity [12,13,14,15,16].

The cubic Laves phase structure of the dialuminides appears to be extremely stable. The low temperature x-ray diffraction (XRD) study of $GdAl_2$ suggests that this compound retains the $MgCu_2$ type structure down to 12 K [17]; the same is true for the pseudo-binary dialuminides, such as $R'_{1-x}Tb_xAl_2$, (R′ = Er, Ho and Tm), that preserve the cubic Laves phase structure down to 5 K [18,19]. To the best of our knowledge, none of the dialuminides formed by either the individual heavy lanthanides (R = Gd – Lu) or their mixtures have been reported to undergo a structural transformation at low temperatures. The only exception is $HoAl_2$, which exhibits an orthorhombic distortion upon spin reorientation transition that occurs in the ferromagnetic state [20]. On the other hand, several of the mixed heavy lanthanide dialuminides exhibit first order like anomalies at low temperature without apparent structural distortions [21]. Compared to the dialuminides formed by heavy lanthanides, much less is known about the low temperature crystallography of the RAl_2 compounds with light lanthanides (R = La and Ce-Eu), even though interesting phenomena have been observed, e.g., heavy fermion behavior and Kondo effect in $CeAl_2$ [22,23].

Another interesting feature of some of the lanthanides is high nuclear specific heat (C_N) contribution at low temperature, which is generally caused by the interactions of the nuclear magnetic moments with the strong magnetic field produced by the 4*f* electrons at the sites of the nuclei, the so-called hyperfine interactions [24]. Additional contribution

to C_N could also result from the nuclear electric quadrupole moment interactions with the electric field gradient [25]. Since the discovery of large nuclear specific heat C_N in terbium [26], the LT C_p (from 0.4 to 4 K) for many other R metals was measured to establish the C_N [24,27]. It was reported that at sufficiently low temperature ($T \leq 2$ K) the Schottky anomaly due to the hyperfine splitting is the dominant term in the total heat capacity of several lanthanides. Despite the fact that LT C_p studies have been carried out for many rare earth systems [28], the detailed nuclear contributions to the total heat capacity of RAl_2 systems have not been studied to date. Magnetic and electrical transport properties, neutron and room temperature x-ray diffraction have been reported for $PrAl_2$ in both the polycrystalline and single crystalline forms [29,30,31,32,33,34,35]. It is well established that $PrAl_2$ is ferromagnetic (FM) with <100> as the easy direction of magnetization [13]. The reported values of Curie temperature (T_C) vary from 30 to 34 K depending upon the sample [33,34,36 and references therein].

In this Letter, we report a remarkable LT structural distortion and the anomalous LT heat capacity of $PrAl_2$ complemented with first principles electronic structure calculations indicating that a strong 4*f* crystal field splitting is responsible for the distorted phase of α-$PrAl_2$ and accounts for the unusual low temperature phenomena.

The polycrystalline $PrAl_2$ alloy was prepared by conventional arc melting of stoichiometric amounts of the constituent elements in an argon atmosphere. The Pr metal was obtained from the Materials Preparation Center of the Ames Laboratory and was 99.98+ wt. % (99.86+ at. %) pure with respect to all other elements in the periodic table

[37]. The Al metal of 4N purity was purchased from Alfa Aeser Inc. Since $PrAl_2$ melts congruently, annealing was not necessary. The crystal structure was determined by powder x-ray diffraction (XRD) experiments performed at temperatures ranging between room temperature and 5 K in zero and applied magnetic fields up to 30 kOe using the x-ray powder diffractometer described in Ref. [38]. The structural parameters were determined from Rietveld analysis using LHPM Rietica [39]. The dc magnetization was measured in a Quantum Design MPMS-XL7 magnetometer. The heat capacity measurements were performed using a homemade adiabatic heat-pulse calorimeter [40] in the temperature range ≈1.8 to 300 K. The physical property measurement system (PPMS by Quantum Design) with ^{3}He option was used to measure the heat capacity from 0.362 to 5 K in magnetic fields up to 140 kOe.

Heat capacity C_p measurements of $PrAl_2$ in various magnetic fields are shown in Fig. 1. The room temperature C_p value is 72.05 J mol^{-1} K^{-1}, which is close to the classical Dulong and Petit limit of the lattice heat capacity at constant volume $C_V = 3nR = 74.83$ J mol^{-1} K^{-1}, where n = 3 is the number of atoms per formula unit and R is the universal gas constant [41]. The value of C_P decreases with decreasing temperature down to the sharp peak at T = 32.5 K, which is due to the paramagnetic (PM) to ferromagnetic (FM) transition [16] . The anomaly in C_p is slightly suppressed upon the application of 1 kOe magnetic field, and it is significantly reduced in height and considerably broadened when applied magnetic field reaches and exceeds 10 kOe. This is the typical behavior of a ferromagnet. The magnetization measurements show that the temperature at which the anomaly observed in zero field C_p data is in an excellent agreement with the PM to FM

transition temperature, T_C = 32.5 K (Fig. 1(a) inset). The ZFC, FCC (or FCW) M(T) curves of $PrAl_2$ show irreversible behavior below T_C. The irreversibility diminishes with the increasing magnetic field and it vanishes when a magnetic field approaches 10 kOe (not shown). Above T_C, magnetic susceptibility follows the Curie-Weiss law. The effective magnetic moment, p_{eff}, and the Weiss temperature, Θ_{pm}, are 3.32 μ_B and 32.6 K, respectively. The observed p_{eff} is slightly lower than the theoretical value $g[J(J+1)]^{1/2}$ = 3.58 μ_B of free Pr^{3+}. The positive value of Θ_{pm} indicates that the ferromagnetic interactions are dominant in $PrAl_2$. The saturation magnetization (M_S) at 2 K is 2.49 μ_B/Pr, which is significantly lower than the theoretical gJ value of 3.2 μ_B for Pr in the ferromagnetic state due to crystalline electric field effects.

In addition to the anomaly at 32.5 K, it is noted that C_p becomes enhanced at T ≤ 4 K, which is clearly seen in the inset of Fig. 1(b). The low temperature C_p of $PrAl_2$ was explored down to 0.36 K in magnetic fields up to 140 kOe (Fig. 1(c)). For comparison, low temperature C_p of pure Pr metal was also measured (Fig. 1(d)). The experimentally measured C_p at T ≤ 2 K for both Pr and $PrAl_2$ were fitted using the following equation

$$C_p = AT^3+BT+C_NT^{-2} \qquad (1)$$

where the first two terms are the standard lattice and electronic contributions, respectively. The third term in Eq. 1 is the contribution from the nuclear specific heat that arises due to the splitting of the nuclear hyperfine levels.

The previously reported zero field C_p of Pr metal below 4 K (Ref. 27) is in considerable disagreement with our data (Fig. 1(d)). Least squares fit of the data for 0.36 K ≤ T ≤ 2 K from Ref. 27 using equation (1) gives nuclear specific heat coefficient C_N = 20.84±0.03 mJ K mol^{-1} which is significantly lower than our C_N = 56.3±0.4 mJ K mol^{-1} at H = 0 kOe. This large difference is not surprising since C_N may greatly be influenced by impurities. The concentrations of major impurities in the Pr metal used in Ref. [27] [in at. %: Fe (0.0038), Ta (0.00156), Ni (0.096), C (0.176), N (0.04), and O (0.097), Na (0.0184)] were at least one order of magnitude higher than the impurity levels in Pr metal used in the present study [in at. %: Fe (0.0006), Ta (0.00006), Ni (0.000098), C (0.019), N (0.036), O (0.082), and Na (0.000031)], except for N and O which were slightly larger. C_N for pure Pr metal increases to 287±2 mJ K mol^{-1} for H = 50 kOe. C_p of $PrAl_2$ at T = 0.364 K and zero magnetic field is an order of magnitude higher than that of pure Pr metal at the same temperature and external magnetic fields. The least squares fit of C_p for α-$PrAl_2$ at H = 0 kOe gives C_N = 624±16 mJ K mol^{-1}, which is significantly higher than the C_N value for Pr metal. The nuclear specific heat coefficients increase with the increasing external magnetic field. Figure 1c inset shows that C_N exhibits two nearly linear dependencies for H≤10 kOe, and H>10 kOe. At low external fields, C_N increases rapidly with a slope of 19.72 mJ K mol^{-1} kOe^{-1}, which correlates with rapidly increasing internal field due to the coalescence of the magnetic domain structure into a single magnetic domain at ~10 kOe; at higher external fields the slope is reduced by an order of magnitude to 1.65 mJ K mol^{-1} kOe^{-1}. The behavior of C_N as a function of external magnetic field indeed follows the behavior of $M(H)$ curve at T = 2 K where magnetization begins to saturate at H≈10 kOe

(not shown in the manuscript). However, it should also be noted that the two linear regions of $C_N(H)$ for $PrAl_2$ may also be related to the crystal field splitting of the tetragonal phase below 10 kOe changing to the crystal field splitting of the cubic structure which is reintroduced by the increasing magnetic field as described below.

An x-ray powder diffraction examination of $PrAl_2$ was performed from room temperature down to 5 K in zero and up to 30 kOe magnetic fields. All powder XRD patterns collected above the magnetic ordering temperature (T_C = 32.5 K) in zero magnetic field show that β-$PrAl_2$ (high temperature polymorph) crystallizes in the Laves phase (cubic $MgCu_2$-type) structure adopting space group $Fd\bar{3}m$. The XRD patterns collected in a zero magnetic field below T_C reflect an unexpected structural distortion that is most noticeable as the splitting of (008) Bragg peak (Fig. 2(a)). The crystal structure below the magnetic ordering temperature (α-$PrAl_2$) becomes tetragonal with space group $I4_1/amd$. However, the splitting of the (008) peak disappears at H = 30 kOe, which signals the recovery of the cubic crystal symmetry (Fig. 2(a-b)).

The temperature dependencies of the lattice parameters in a zero magnetic field and in 30 kOe field are presented in Fig. 2(c). While cooling, the cubic phase contracts nearly linearly with the linear thermal expansion coefficient of $\approx 1.2\times10^{-5}$ K^{-1}, but below T_C the lattice rapidly expands nonlinearly along the four-fold axis while it contracts in a similar fashion in the basal plane of the tetragonal structure. Despite the relatively sharp peak in C_p at 32.5 K, the unit cell volume changes continuously (Fig. 2(c) inset), suggesting that

thermodynamically the magnetostructural transition at T_C is a second order transformation, which is consistent with the heat capacity data shown in Fig. 1(a) and 1(b). The increase of the unit cell value below T_C at 30 kOe is related to the conventional magnetostriction reaching ~1,000 ppm for $\frac{\Delta a}{a}$ at 5 K. The field dependencies of the lattice parameters at T = 12 K show clear evidence of tetragonal distortion below 10 kOe (Fig. 2(d)). The increasing magnetic fields drive the tetragonal phase to the parent cubic phase when H≥10 kOe (see Fig. 2(d)), and both the cubic and tetragonal phases co-exist in 1 kOe to 10 kOe magnetic fields (see inset b of Fig. 2(d)). The magnetic field-induced tetragonal to cubic phase transformation which occurs below 30 K is reversible: upon removal of the magnetic field at 12 K, the cubic phase stabilized by a 30 kOe field transforms to the original tetragonal phase stable at zero field (not shown in Fig. 2d for clarity).

In order to clarify the origin of both the structural distortion and the low temperature anomaly in the specific heat of $PrAl_2$, we carried out density functional theory (DFT) calculations using local spin density approximation (the von Barth-Hedin exchange correlation potentials) with the *U* correction (Coulomb repulsion between 4*f* electrons), LSDA+*U* approach [42]. This approach takes into account orbital dependency of *U* and *J* (exchange interaction between localized 4*f* electrons) and is implemented in the tight binding linear muffin tin orbital (TB-LMTO) [43] band structure method. *U* =6.7 eV and *J*=0.7 eV, which are well known for Gd, were used to model the strong electron

correlation parameters for Pr in FM $PrAl_2$ considering the similar energy difference between the occupied and unoccupied 4*f* states.

The total energy of the tetragonal FM α-$PrAl_2$ is lower by 16.8 meV/cell compared to the total energy of the cubic FM β-$PrAl_2$, which confirms the experimentally observed low temperature tetragonal distortion in this material. The calculated magnetic moment of Pr in α-$PrAl_2$ for the ferromagnetic tetragonal structure is 2.36 μ_B/Pr (5 μ_B/Pr from 4*f* orbitals, 2.49 μ_B/Pr from the 4*f* spins and 0.15 μ_B/Pr from conduction electron spins), which is in close agreement with the experimentally observed value of 2.49 μ_B/Pr at 2 K.

Figure 3 shows the 4*f* and 5*d* density of states of Pr and 3*p* density of states of Al near the Fermi level in the cubic (β) and the tetragonally distorted (α) Laves phases of $PrAl_2$. The unoccupied spin up and spin down 4*f* states located well above the Fermi level in both of the structures are not shown here. The Al 3*p* densities of states are strongly hybridized with Pr 5*d* resulting in a small but non negligible moment in Al 3*p* in both structures. The spin up 4*f* density of states in the cubic structure is centered at two energy locations ~0 eV and ~-0.5 eV. On the other hand, the spin up 4*f* density of states in the tetragonally distorted structure is centered mainly in three energy locations ~0 eV, ~-0.32, and -1.7 eV. This shows that the tetragonally distorted phase exhibits crystal field splitting of ~1 eV, which apparently makes the tetragonally distorted phase the ground state as confirmed from the total energy calculations.

The 4*f* bands, located at ~0 eV, ~-0.32 eV in the tetragonal structure, hybridize with the corresponding 5*d* bands giving rise to 5*d* density of states peaks around the Fermi level, supporting 4*f*-5*d* exchange interactions similar to those in the cubic $PrAl_2$. Because of the 4*f* band splitting in the tetragonal structure, the 4*f* bands, located at ~-1.7 eV, also hybridize with the corresponding 5*d* bands thus providing an additional 4*f*-5*d* contribution to exchange interactions compared to the cubic $PrAl_2$. As the 4*f* crystal field splitting increases, the cubic $PrAl_2$ orders ferromagnetically and distorts to the tetragonal structure, thus linking the ferromagnetic state to the tetragonal distortion through the 4*f* crystal field splitting. With the application of magnetic field, which directly interacts with the localized 4*f* spin and affects conduction electrons by inducing a polarization in the conduction band, the indirect 4*f*-4*f* exchange interactions increase [44], and the extra 4*f* crystal field splitting is lifted; as a result the distorted structure changes to the original cubic structure.

The total energy of the double hexagonal structure with antiferromagnetic configuration of elemental Pr is lower by 0.53 meV compared to the ferromagnetic counterpart indicating that an antiferromagnetic state here is the ground state. Interestingly, the experimentally reported antiferromagnetic transition of Pr is close to 0 K. Since degenerate occupied 4*f* bands lie well below the Fermi level (Fig. 4), it is not surprising that the aspherical 4*f* charge density having local 4*f* spin moment of 2 μ_B/Pr may couple to its nuclear counterpart, which is several orders of magnitude smaller than the 4*f* spin moment, via the conduction electron spins (0.15 μ_B/Pr) leading to modification of the

energy levels of the nuclear spin system [45]. This nuclear hyperfine coupling gives rise to anomaly in the specific heat close to 0 K in the double hexagonal Pr.

The local spin moment, 2.64 μ_B/Pr (2.49 μ_B/Pr from the 4*f* spins and 0.15 μ_B/Pr from conduction electron spins), is stronger in FM α-$PrAl_2$ compared to the local spin moment, 2.15 μ_B/Pr, (2 μ_B/Pr from the 4*f* spins and 0.15 μ_B/Pr from conduction electron spins) in the elemental AFM Pr. It is well known that nuclear spins interact with one other through indirect 4*f*-4*f* exchange interactions, commonly known as RKKY (Ruderman-Kittel-Kasuya-Yosida) interactions. Although the calculated 5*d* spin polarizations are the same (0.15 μ_B/Pr) in the tetragonal $PrAl_2$ and hexagonal Pr, they are positive in the former and negative in the latter due to different crystallography and different Pr-Pr distances, thus resulting in the stronger nuclear hyperfine interactions in $PrAl_2$ compared to metallic Pr. Moreover there is a strong 4*f* crystal field splitting in $PrAl_2$. This should further modify the nuclear energy levels leading to a stronger nuclear hyperfine splitting and giving rise to an order of magnitude higher Schottky specific heat peak close to 0 K in $PrAl_2$ compared to the elemental Pr.

In conclusion, we report abnormally high Schottky specific heat in $PrAl_2$, an order of magnitude higher than that of pure Pr. The low temperature XRD demonstrates that the FM transition in $PrAl_2$ at T_C is accompanied by a structural transformation from the cubic to the tetragonal crystal structure with a continuous volume change. . The cubic symmetry is fully recovered with the application of magnetic field of 10 kOe and higher by lifting the 4*f* crystal field splitting. The strong 4*f* splitting and the 4*f* density of states

peak at the Fermi level established from the first principles calculations confirm the low temperature anomaly and the structural distortion below T_C. The modification of the energy levels of the nuclear spin system due to the 4*f* band splitting gives rise to additional nuclear hyperfine splitting resulting in higher Schottky specific heat close to 0 K in α-$PrAl_2$ compared to the elemental Pr.

This work was supported by the Office of Basic Energy Sciences, Division of Material Sciences and Engineering of the U.S. Department of Energy under contract No. DE-AC02-07CH11358 with Iowa State University of Science and Technology.

Figure Captions:

FIG. 1 (color online) (a) The heat capacity of $PrAl_2$ measured in different external magnetic fields. The inset shows zero field cooled (ZFC) warming, field cooled cooling (FCC), and field cooled warming (FCW) magnetization of $PrAl_2$ measured in H = 100 Oe. (b) The C_p/T as a function of T^2. The inset shows the details at low-temperature. (c) The heat capacity of α-$PrAl_2$ measured below 5 K in different magnetic fields. (d) The heat capacity of Pr metal measured below 5 K in different magnetic fields. The insets in c and d show nuclear specific heat coefficients C_N (from the fits of data for 0.6 K ≤ T ≤ 2 K to Eq.1) as functions of applied magnetic field. The solid triangle in the inset d represents the data from Ref. [27]. The solid lines in (c) and (d) are the fits of the data to Eq.1 for T ≤ 2 K. The errors in C_N are about the size of the symbols.

FIG. 2 (color online) The intensity contour map of the x-ray diffraction patterns of $PrAl_2$ measured in H = 0 kOe (a) and H = 30 kOe (b). (c) The unit-cell dimensions of $PrAl_2$ as a function of temperature at H = 0 and 30 kOe. The inset in (c) shows the phase volume as a function of temperature at H = 0 and 30 kOe. (d) The unit-cell dimensions of $PrAl_2$ as a function of field at T = 12 K measured in increasing magnetic field. The insets (a) and (b) of Fig. (d) show, respectively, the phase volumes and the concentrations of the cubic and tetragonal phases as functions of field. The solid lines are guides to the eye.

FIG. 3 (color online) The 4*f* and 5*d* density of states of Pr and 3*p* density of states of Al in the cubic (β) (a) and tetragonally distorted (α) (b) Laves phases of $PrAl_2$.

FIG. 4 (color online) The 4*f* and 5*d* density of states of the antiferromagnetic Pr in double hexagonal structure.

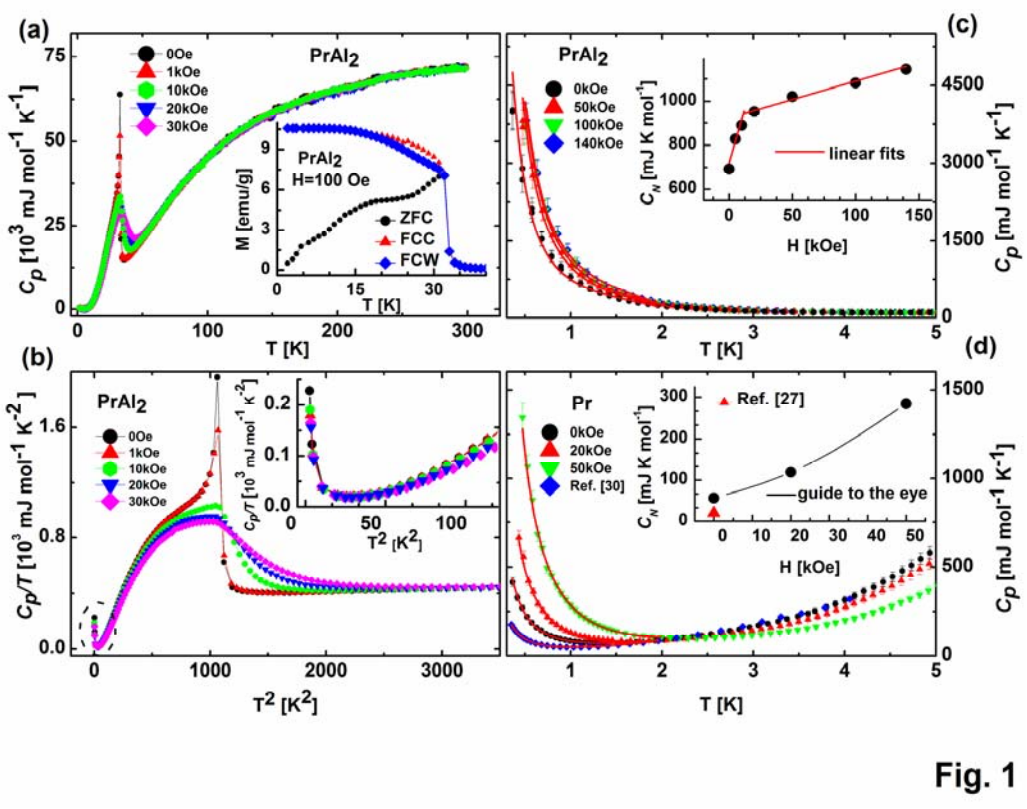

Fig. 1

FIG. 1 (color online) (a) The heat capacity of $PrAl_2$ measured in different external magnetic fields. The inset shows zero field cooled (ZFC) warming, field cooled cooling (FCC), and field cooled warming (FCW) magnetization of $PrAl_2$ measured in H = 100 Oe. (b) The C_p/T as a function of T^2. The inset shows the details at low-temperature. (c) The heat capacity of α-$PrAl_2$ measured below 5 K in different magnetic fields. (d) The heat capacity of Pr metal measured below 5 K in different magnetic fields. The insets in c and d show nuclear specific heat coefficients C_N (from the fits of data for 0.6 K ≤ T ≤ 2 K to Eq.1) as functions of applied magnetic field. The solid triangle in the inset d represents the data from Ref. [27]. The solid lines in (c) and (d) are the fits of the data to Eq.1 for T ≤ 2 K. The errors in C_N are about the size of the symbols.

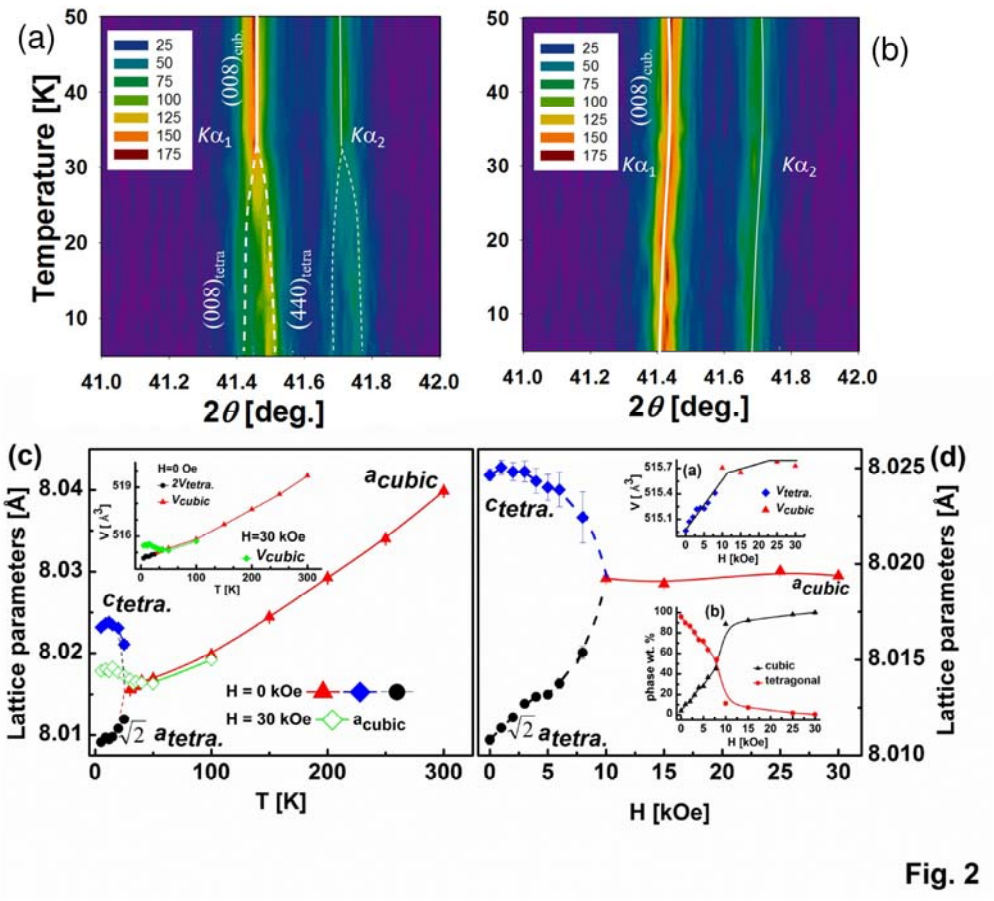

Fig. 2

FIG. 2 (color online) The intensity contour map of the x-ray diffraction patterns of $PrAl_2$ measured in H = 0 kOe (a) and H = 30 kOe (b). (c) The unit-cell dimensions of $PrAl_2$ as a function of temperature at H = 0 and 30 kOe. The inset in (c) shows the phase volume as a function of temperature at H = 0 and 30 kOe. (d) The unit-cell dimensions of $PrAl_2$ as a function of field at T = 12 K measured in increasing magnetic field. The insets (a) and (b) of Fig. (d) show, respectively, the phase volumes and the concentrations of the cubic and tetragonal phases as functions of field. The solid lines are guides to the eye.

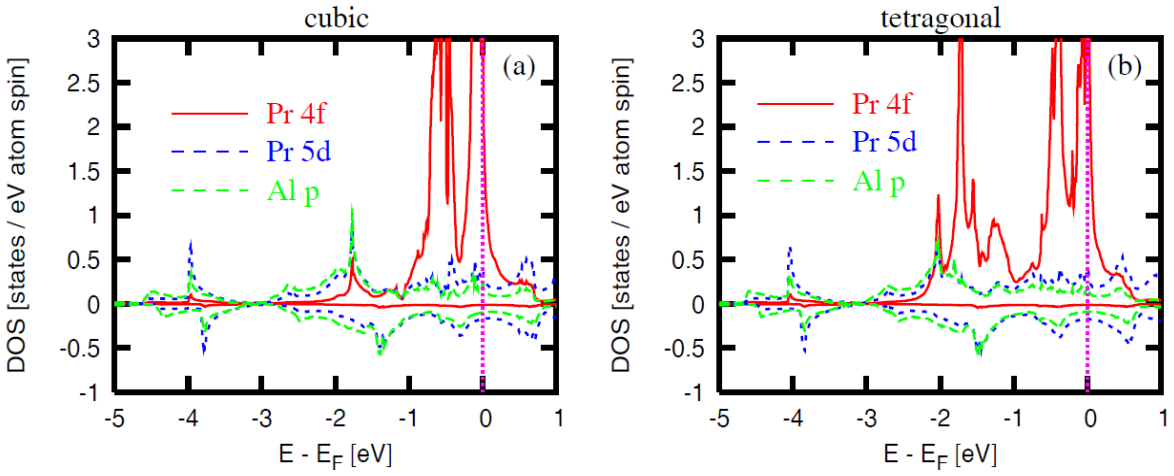

Fig. 3 (color online) The 4*f* and 5*d* density of states of Pr and 3*p* density of states of Al in the cubic (β) (a) and tetragonally distorted (α) (b) Laves phases of $PrAl_2$.

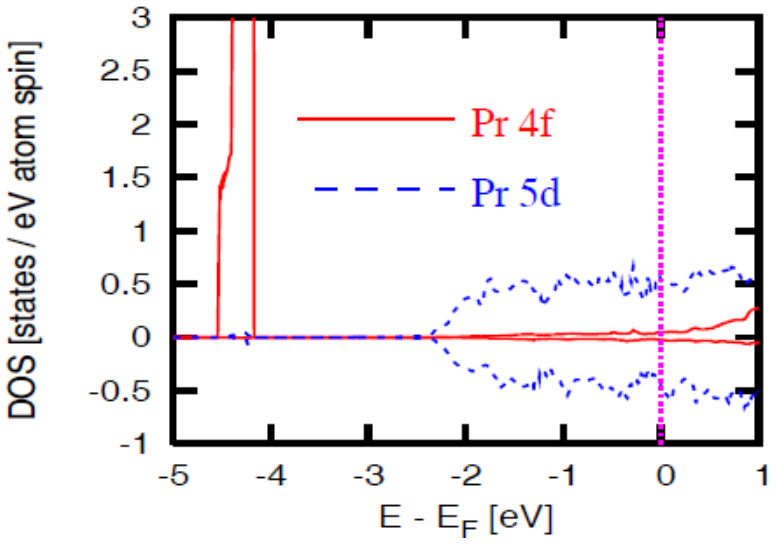

FIG. 4 (color online) The 4*f* and 5*d* density of states of the antiferromagnetic Pr in double hexagonal structure.

References:

[1] S. Jin, T. H. Tiefel, M. McCormack, R. A. Fastnacht, R. Ramesh and L. H. Chen, Science **264**, 413 (1994).

[2] K. Ullakko, J. K. Huang, C. Kantner, R. C. O'Handley, and V. V. Kokorin, Appl. Phys. Lett. **69**, 1966 (1996).

[3] O. Tegus, E. Brück, K. H. J. Buschow and F. R. de Boer, Nature **415**, 150 (2002).

[4] V. K. Pechasky, A. P. Holm, K. A. Gschneidner, Jr., and R. Ring, Phys. Rev. Lett. **91**, 197204 (2003).

[5] J. Zhao, Q. Huang, C. de la Cruz, S. Li, J. W. Lynn, Y. Chen, M. A. Green, G. F. Chen, G. Li, Z. Li, J. L. Luo, N. L. Wang, and P. Dai, Nature Materials **7,** 953 (2008).

[6] A. Asamitsu, Y. Moritomo, R. Kumai, Y. Tomioka, and Y. Tokura, Phys. Rev. B **54**, 1716 (1996).

[7] J. Stankiewicz, M. Evangelisti, Z. Fisk , P. Schlottmann, and Lev P. Gor'kov, Phys. Rev. Lett. **108**, 257201 (2012)**.**

[8] T. Brugger, T. Schreiner, G. Roth, P. Adelmann, and G. Czjzek, Phys. Rev. Lett. **71**, 2481 (1993).

[9] A. V. Chubukov, S. Sachdev, and J. Ye, Phys. Rev. B **49**, 11919 (1994).

[10] H. K. Collan, M. Krusius, and G. R. Pickett, Phys. Rev. B **1**, 2888 (1970)

[11] J. H. Wernick, and S. Geller, Trans. AIME **218**, 866 (1960).

[12] H. G. Purwins, and A. Leson, Advances in Physics **39**, 309 (1990).

[13] H. G. Purwins, E. Walker, B. Barbara, M. F. Rossignol, and P. Bak, J. Phys: C: Solid State. Phys. **7**, 3573 (1974).

[14] P. J. von Ranke, V. K. Pecharsky, and K. A. Gschneidner, Jr., Phys. Rev. B **58**, 12110 (1998).

[15] D. J. Goossens, S. J. Kennedy, T. J. Hicks, Nuclear Inst. and Methods in Phys. Res. A 390, 572 (1996).

[16] Th. Frauenheim, W. Matz, and G. Feller, Solid State Commun, **29**, 805 (1979).

[17] T. Oishi, M.Ohashi, H. Suzuki, and I. Satoh, J. Phys.: Conf. Series **200**, 082022 (2010).

[18] M. Khan, Ya. Mudryk, K. A. Gschneidner Jr., and V. K. Pecharsky, Phys. Rev. B **84**, 214437 (2011).

[19] M. Khan, Ya. Mudryk, D. Paudyal, K. A. Gschneidner Jr., and V. K. Pecharsky, Phys. Rev. B **82**, 064421 (2010).

[20] M. R. Ibarra, O. Moze, P. A. Algarabel, J. I. Arnaudas, J. S. Abell, and A. del Moral, J. Phys. C: Solid State. Phys. **21**, 2735 (1988).

[21] M. Khan, D. Paudyal, Y. Mudryk, K. A. Gschneidner, Jr. and V. K. Pecharsky, Phys. Rev. B **83**, 134437 (2011).

[22] Y. Onuki, Y. Furukawa, T. Komatsubara, J. Phys. Soc. Jpn. **53** 2734, (1984).

[23] H. Miyagawa, G. Oomi, M. Ohashi, I. Satoh, T. Komatsubara, M. Hedo, Y. Uwatoko, Phys. Rev.B **78**, 064403 (2008).

[24] O. V. Lounasmaa, and R. A. Guenther, Phys. Rev. **126**, 1357 (1962).

[25] B. Bleaney and R. W. Hill, Proc. Phys. Soc. (London) **78**, 313 (1961).

[26] N. Kurti, and R. S. Safrata, Phil. Mag. **3**, 780 (1958).

[27] O. V. Lounasmaa, Phys. Rev. **133**, A211 (1964), Phys. Rev. **129**, 2460 (1963), Phys. Rev. **133**, A219 (1964), Phys. Rev. **126**, 1352 (1962).

[28] M. J. McDermott, and K. K. Marklund, J. Appl. Phys. **40**, 1007 (1969).

[29] L. Palermo, and X. A. Da Silva, Phys. Stat.Sol. (b) **103**, 419 (1981).

[30] N. Kaplan, E. Dormann, K. H. J. Buschow, and D. Lebenbaum, Phys. Rev. B **7**, 40 (1973).

[31] K. Henning, L. P. Kaun, B. Lippold, S. Matthies, W. Matz, W. Drexel, P. Seifert, and Moreva, Solid State Commun. **21**, 297 (1977).

[32] R. J. Lange, S. J. Lee, K. J. Kim, P. C. Canfield, and D. W. Lynch, Phys. Rev. B **63**, 035105 (2000).

[33] J. C. P. Campoy, E. J. R. Plaza, A. A. Coelho, and S. Gama, Phys. Rev. B **74**, 134410 (2006).

[34] N. Nereson, C. Olsen, and G. Arnold, J. Appl. Phys. **39**, 4605 (1968).

[35] A. Eyers, A. Alke, A. Leson, D. Kohake, and H. G. Purwins, J. Phys. C: Solid State Phys. **15**, 2459 (1982).

[36] A. Magnus G. Carvalho, J. C. P. Campoy, A. A. Coelho, E. J. R. Plaza, S. Gama, and P. J. von Ranke, J. Appl. Phys. **97**, 083905 (2005).

[37] Materials Preparation Center, Ames Laboratory of US, DOE, Ames, IA, USA, www.mpc.ameslab.gov.

[38] A. P. Holm, V. K. Pechasky, K. A. Gschneidner, Jr., R. Ring, and M. Jirmanus, Rev. Sci. Instrum. **75**, 1081 (2004).

[39] B. Hunter, Rietica-A Visual Rietveld Program, International Union of Crystallography Commission on Powder Diffraction Newsletter No. 20, (Summer, 1998) [http://www.rietica.org].

[40] V. K. Pecharsky, J. O. Moorman, and K. A. Gschneidner Jr., Rev. Sci. Instrum. **68**, 4196 (1997).

[41] C. Kittel, *Introduction to Solid State Physics* (Wiley, New York), 8th ed. (2005).

[42] V. I. Anisimov, F. Aryasetiawan, and A. I. Lichtenstein, J. Phys.: Condens. Matter. **9**, 767 (1997).

[43] O. K. Andersen and O. Jepsen, Phys. Rev. Lett. **53**, 2571 (1984).

[44] T. Balcerzak, Phys. Stat. sol. (c) 3, 212 (2006).

[45] A. Abragam, *The Principles of Nuclear Magnetism*, (Oxford University Press, London) (1961).